Reduction of Cogging Torque and Electromagnetic Vibration Based on Different Combination of Pole Arc Coefficient for Interior Permanent Magnet Synchronous Machine

Feng Liu, Xiuhe Wang, *Member, IEEE*, Zezhi Xing, Aiguo Yu, and Changbin Li

***Abstract*—Cogging torque and electromagnetic vibration are two important factors for evaluating permanent magnet synchronous machine (PMSM) and are key issues that must be considered and resolved in the design and manufacture of high-performance PMSM for electric vehicles. A fast and accurate magnetic field calculation model for interior permanent magnet synchronous machine (IPMSM) is proposed in this article. Based on the traditional magnetic potential permeance method, the stator cogging effect and complex boundary conditions of the IPMSM can be fully considered in this model, so as to realize the rapid calculation of equivalent magnetomotive force (MMF), air gap permeance, and other key electromagnetic properties. In this article, a 6-pole 36-slot IPMSM is taken as an example to establish its equivalent solution model, thereby the cogging torque is accurately calculated. And the validity of this model is verified by a variety of different magnetic pole structures, pole slot combinations machines, and prototype experiments. In addition, the improvement measure of the machine with different combination of pole arc coefficient is also studied based on this model. Cogging torque and electromagnetic vibration can be effectively weakened. Combined with the finite element model and multi-physics coupling model, the electromagnetic characteristics and vibration performance of this machine are comprehensively compared and analyzed. The analysis results have well verified its effectiveness. It can be extended to other structures or types of PMSM and has very important practical value and research significance.**

***Index Terms*—Cogging torque, different combination of pole arc coefficient, electromagnetic vibration, interior permanent magnet synchronous machine.**

I. Introduction

With the increasingly severe environmental problems and energy situation, new energy vehicles are gradually replacing traditional fuel vehicles to become the trend of future automotive development [1]. Among them, electric vehicles have received extensive attention and the machine is considered to be the key component of its electric drive system. In recent years, permanent magnet synchronous machine (PMSM) has broad application prospects in the field of electric drives due to its high power/torque density, high efficiency, and high reliability [2][3]. Compared with surface-mounted PMSM, interior permanent magnet synchronous machine (IPMSM) is more popular due to its superior electromagnetic characteristics such as wide speed range and high overload capacity [4][5]. It is worth mentioning that, for IPMSM, the torque ripple and electromagnetic vibration caused by cogging, reluctance and permanent magnet (PM) torque have always been thorny issues restricting its further development [6]. Especially when electric vehicles are running under complex operating conditions, these defects tend to cause electromagnetic mechanical problems such as irreversible demagnetization, low output torque/power, temperature rise, bearing wear, and noise. Therefore, the research on cogging torque and electromagnetic vibration of IPMSM is particularly important in its design stage [7].

The numerical calculation method represented by finite element method (FEM) and the analytical method represented by magnetic circuit method, equivalent surface current method, and subdomain method are the main methods to analyze the key electromagnetic characteristics of PMSM such as cogging torque. The influence of the complex structure, saturation, temperature rise, and magnetic flux leakage can be fully considered in FEM, which has good calculation accuracy [8]. However, a lot of computing resources and time need to be consumed, and the internal correspondence between electromagnetic characteristics and structural parameters is difficult to be accurately analyzed, which is not conducive to the optimization from the mechanism. In recent years, various analysis methods have emerged one after another. A magnetic equivalent circuit model of the AC homopolar machine for flywheel energy storage is proposed, which greatly shortens the calculation time [9]. An improved equivalent surface current method for surface-mounted PMSM is developed [10]. Combining the subdomain model and vector magnetic potential superposition method, the mutual transformation between the

Manuscript received October 06, 2021; revised November 03, 2021; accepted December 01, 2021. date of publication December 25, 2021; date of current version December 18, 2021.

This work was supported in part by the National Natural Science Foundation of China under Grant 51737008. (*Corresponding author: Xiuhe Wang.*)

Feng Liu, Xiuhe Wang, Zezhi Xing, and Changbin Li are with the School of Electrical Engineering, Shandong University, Jinan 250061, China (e-mail: liucf1019@163.com; wangxh@sdu.edu.cn; xzz_sd001@163.com; ChangbinL@163.com).

Aiguo Yu is with the Qingdao Haidian Electric Co. Ltd, Qingdao 266109, China (e-mail: 13605320256@126.com).

Digital Object Identifier 10.30941/CESTEMS.2021.00034

local and global coordinate systems is adopted, which avoids calculation complexity. In addition, the precise subdomain method is widely used in the calculation of spoke-type PMSM [11], surface-mounted PMSM [12], PMSM with rotor eccentric [13], and other machines due to its high accuracy. It is undeniable that the existing analytical methods are still mainly applicable to surface-mounted PMSM, and their applicability to IPMSM is still limited by its complex structure, and it is often necessary to sacrifice calculation accuracy to meet the prerequisites. And preliminary modeling work for different structures often requires a lot of time.

Many scholars have done a lot of research on the reduction and improvement of cogging torque and electromagnetic vibration for IPMSM [14]. Effective reduction measures such as unequal tooth width [15], harmonic pole-cutting [16], magnetic pole offset [17], pole arc coefficient selection [18], and adding auxiliary slots [19] have been proposed one after another. Stator skew slots and rotor skew poles are very popular among researchers in IPMSM for electric vehicles [20]. However, they have been criticized for their machining difficulties and electromagnetic sacrifices. Similarly, the machine with "\"-type, "V"-type, and "Z"-type rotor skew poles will also introduce unbalanced magnetic pulling force, which in turn will cause electromagnetic vibration and shorten its life [21]. In addition, the electromagnetic excitation force wave, as another main factor of vibration, needs to be studied while weakening the torque ripple caused by cogging torque. Especially for the design of IPMSM for electric vehicles, not only the influence of low-order excitation force wave amplitude on electromagnetic vibration and mechanical life, but also the electromagnetic magnetic resonance phenomenon caused by excitation force wave and natural frequency of the same order vibration mode are considered [22].

To solve the aforementioned conflicts, a magnetic field calculation model suitable for IPMSM is first given in Section II. Based on traditional magnetic permeance method, the stator cogging effect and the influence of complex boundary conditions can be fully considered in this model, so as to achieve the fast calculation of equivalent magnetomotive force (MMF), equivalent air gap permeance/effective air gap length, and other key electromagnetic properties. Its accuracy, universality, and feasibility have been verified through FEM and prototype experiments. After that, based on this model, the improvement measure using different combination of pole arc coefficient is studied in Section III, and the cogging torque and electromagnetic vibration of IPMSM are effectively weakened. The electromagnetic characteristics, vibration performance, and mechanical strength of this machine are comprehensively compared and analyzed in Section IV, and the effectiveness and rationality of this improvement has been well proved.

II. Analysis and Verification of Cogging Torque

A. Accurate Analytical Model of Cogging Torque

Cogging torque is an inherent property of the PMSM, which is defined as the negative derivative of the magnetic field energy W with respect to the relative position angle α of stator and rotor when the machine is not energized. So, it can be expressed as

$$T_{\text{cog}} = -\frac{\partial W}{\partial \alpha} \tag{1}$$

Fig. 1 illustrates the stator and rotor configuration of a 6-pole 36-slot 7.5kW V-shaped IPMSM. The analysis model of this machine under one specific magnetic pole is shown in Fig. 2. In this figure, θ represents the rotor position angle, θ=0° represents the centerline of this specific magnetic pole, and the angle between the centerline of one stator tooth (A-phase axis) and the centerline of this specific magnetic pole is defined as α (that is, relative position angle of the stator and rotor). In addition, the main structural parameters and configuration description of this machine are shown in Table I.

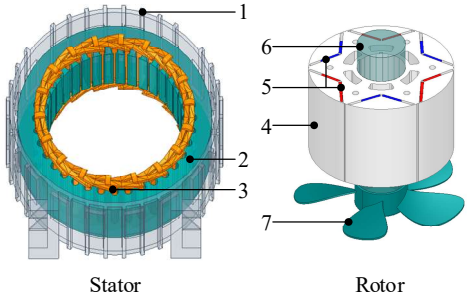

Fig. 1. Schematic diagram of stator and rotor in the IPMSM, 1-housing, 2-stator core, 3-winding, 4-rotor core, 5-PMs, 6-shaft, 7-fan.

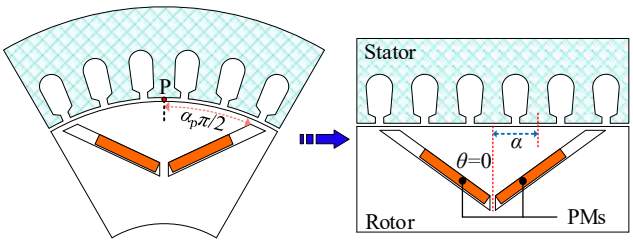

Fig. 2. Relative position of stator and rotor in the IPMSM.

TABLE I
THE MAIN PARAMETERS DESCRIPTION OF IPMSM

Item	Value (unit)
Outer diameter of stator core	260 (mm)
Inner diameter of stator core	180 (mm)
Outer diameter of rotor core	179 (mm)
Inner diameter of rotor core	60 (mm)
Number of stator teeth	36 (/)
Rated torque	71.63 (N·m)
Rated power	7.5 (kW)
Rated frequency	50 (Hz)
Rated speed	1000 (rpm·min^{-1})
Remanence of PM	1.19 (T)
Coercivity of PM	857 (kA·m^{-1})
Number of pole pairs	3 (/)

Considering that the core magnetic permeability is infinite, the magnetic field energy stored in this machine can be expressed as

$$\begin{aligned} W &\approx W_{\text{ag}} \\ &= \frac{1}{2\mu_0}\int_V B_{\text{ag}}^2(\theta,\alpha)\,\mathrm{d}V \\ &= \frac{\mu_0}{2}\int_V F^2(\theta)\Lambda^2(\theta,\alpha)\,\mathrm{d}V \end{aligned} \tag{2}$$

where W_{ag} represents the air gap magnetic field energy storage, μ_0 represents the air gap permeability, $B_{ag}(\theta,\alpha)$ represents the air gap flux density distribution, $F(\theta)$ and $\Lambda(\theta,\alpha)$ are the equivalent permanent MMF and air gap permeance, respectively.

Therefore, the key to accurately calculate the cogging torque lies in the analysis of $F(\theta)$ and $\Lambda(\theta,\alpha)$. Detailed analysis flow chart is shown in Fig. 3.

First, the machine model without stator cogging structure (Fig. 4(a)) is selected to calculate $F(\theta)$. Considering that the stator inner surface and rotor outer surface are smooth planes, the air gap length is a certain value δ_0, and the magnetic pressure drop of the stator and rotor cores can be ignored, so the air gap MMF $F_\delta(\theta)$ can be approximately equivalent to permanent MMF $F(\theta)$, namely

$$F(\theta) = B_0(\theta)\frac{\delta_0}{\mu_0} \tag{3}$$

where $B_0(\theta)$ represents the air gap flux density distribution ignoring stator slots. Therefore, the Fourier expansion of $F^2(\theta)$ on half an electrical period $[-\pi/2p, \pi/2p]$ can be expressed as

$$F^2(\theta) = F_0 + \sum_{n=1}^{\infty} F_n \cos 2np\theta \tag{4}$$

where p represents the number of pole pairs. F_0 and F_n represent the Fourier expansion coefficients.

Furthermore, to consider the influence of the complex cogging structure, the machine model with stator slots (Fig. 4(b)) is selected to calculate $\Lambda(\theta,\alpha)$. Considering that the magnetic resistance of stator core is much smaller than that of air gap, its outer surface can be regarded as an isomagnetic potential surface within the entire pitch range, so the corresponding MMF $F_{\delta t}$ can be obtained by

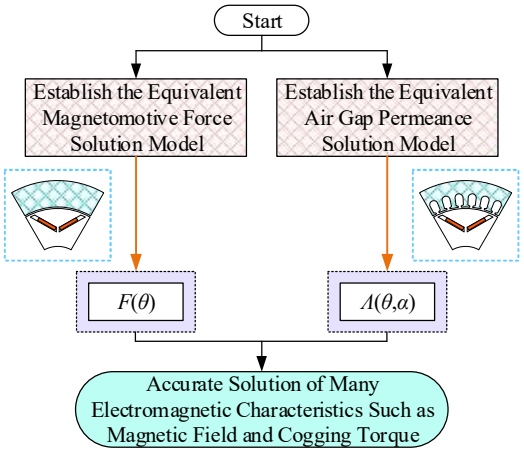

Fig. 3. Flow chart of the analytical model for IPMSM.

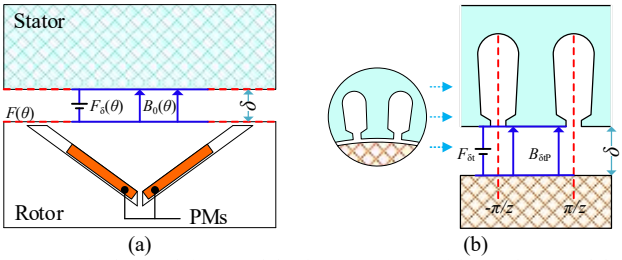

Fig. 4. Equivalent solving model of IPMSM (a: without slots model for equivalent MMF, b: with slots model for equivalent air gap permeance).

$$F_{\delta t} = B_{\delta tP}\frac{\delta_0}{\mu_0} \tag{5}$$

where $B_{\delta tP}$ represents the flux density corresponding to the measurement point P (Fig. 2) at one stator tooth center. Therefore, the effective air gap length $\delta(\theta,\alpha)$ can be obtained by

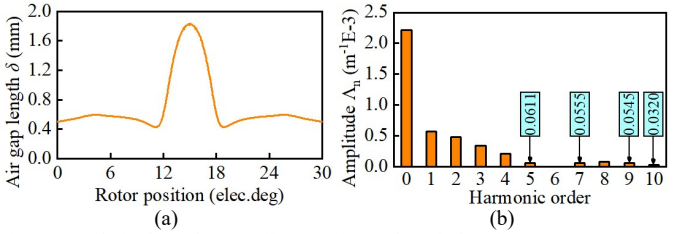

Fig. 5. Analytical results (a: Effective air gap length, b: Air gap permeance).

$$\delta(\theta,\alpha) = \mu_0\frac{F_{\delta t}}{B_{\delta t}(\theta,\alpha)} \tag{6}$$

where $B_{\delta t}(\theta,\alpha)$ represents the air gap flux density distribution within one tooth pitch range. Similarly, the Fourier expansion of $\Lambda^2(\theta,\alpha)$ in a range of tooth pitch can be expressed as

$$\Lambda^2(\theta,\alpha) = \Lambda_0 + \sum_{j=1}^{\infty}\Lambda_j \cos jz(\theta+\alpha) \tag{7}$$

where z represents the number of stator teeth, Λ_0 and Λ_n represent the Fourier expansion coefficients. Based on the aforementioned analysis, the calculation results of the effective air gap length $\delta(\theta,\alpha)$ and the corresponding components of the air gap permeance $\Lambda(\theta,\alpha)$ for this machine are shown in Fig. 5.

Combining (1), (4) and (7), the cogging torque analytical expression of the IPMSM can be expressed as

$$T_{cog} = \frac{\mu_0\pi z L_{ef}}{4}\left(R_{s2}^2 - R_{r1}^2\right)\sum_{j=1}^{\infty} j\Lambda_j F_n \sin jz\alpha \tag{8}$$

where L_{ef} represents the axial length, R_{r1} represents the rotor outer diameter, R_{s2} represents the stator inner diameter, and j and n represent positive integers satisfying $n=jz/2p$. In addition, many electromagnetic characteristics, such as air gap flux density, no-load back EMF, and electromagnetic force wave, can also be quickly and accurately calculated by this model.

B. Analytical Model Verification and Experiment Testing

1) Different magnetic pole structure

Aiming at the commonly used magnetic pole structures of the IPMSM for electric vehicles, three magnetic pole structures (U-shaped, V-shaped, and one-shaped) are compared and analyzed. Three magnetic pole structures are shown in Fig. 6. The comparison of cogging torque and flux density calculated by the FEM and analytical method are shown in Fig. 7.

It is not difficult to find that the air gap flux density calculated by the two methods have an excellent agreement. In addition, the peak-to-peak cogging torque calculated by the two methods for U-shaped, V-shaped, and one-shaped machines are 6.45N·m and 6.13N·m, 7.64N·m and 7.18N·m, 8.59N·m and 8.07N·m, calculation errors of the three machines are only 5.00%, 6.02%, and 6.05%. The universality and accuracy of this model are well proven.

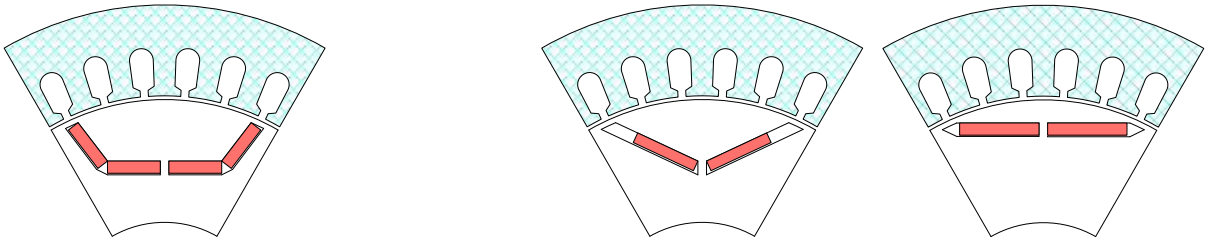

(a) "U"-type (b) "V"-type (c) "—"-type

Fig. 6. Machine topology with different magnetic pole structures.

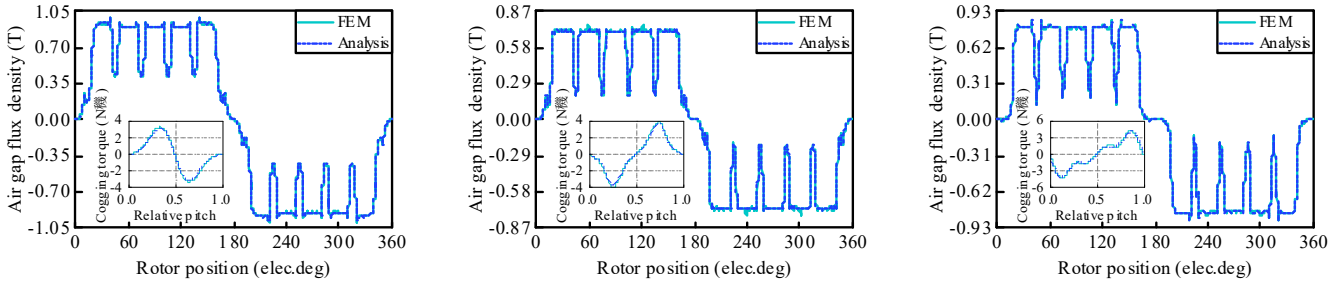

(a) "U"-type (b) "V"-type (c) "—"-type

Fig. 7. Comparison of electromagnetic characteristics for the machine with different magnetic pole structure.

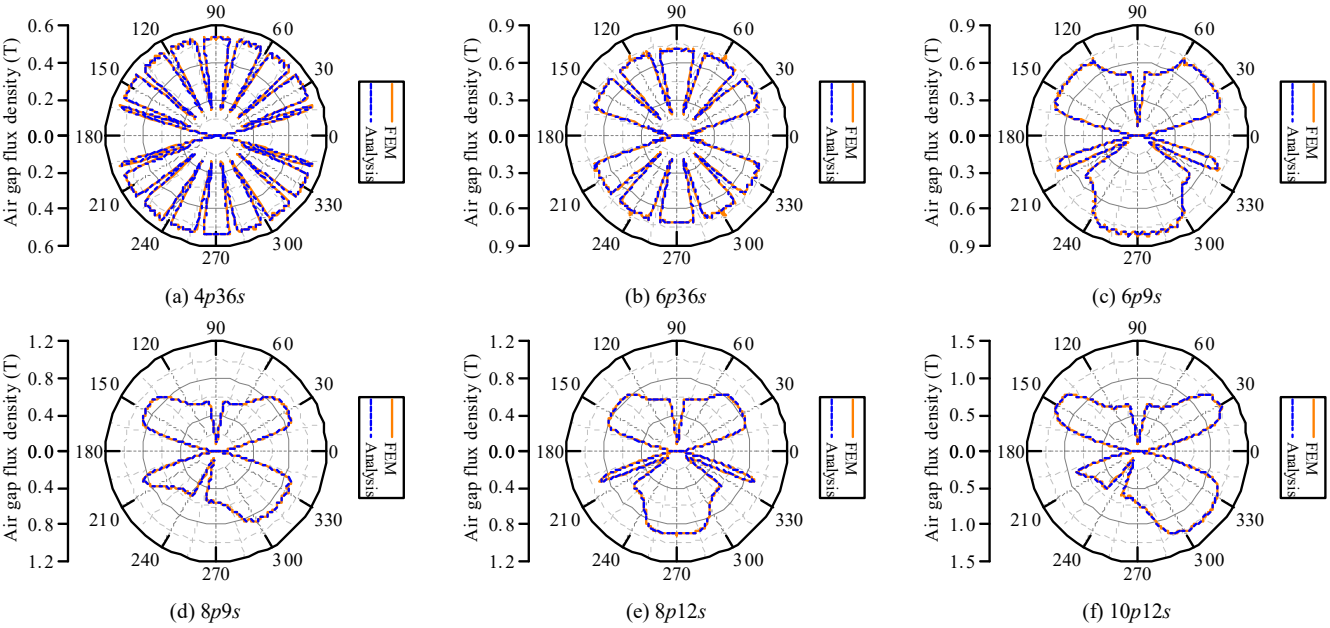

(a) 4*p*36*s* (b) 6*p*36*s* (c) 6*p*9*s*

(d) 8*p*9*s* (e) 8*p*12*s* (f) 10*p*12*s*

Fig. 8. Comparison of air gap flux density for the machine with different pole-slot combination.

2) Different pole-slot combination

Theoretically, the proposed analytical model is also applicable to machine with any pole-slot combination including IPMSM. Therefore, in order to verify its versatility, six V-shaped IPMSM with different pole-slot combinations (4*p*36*s*, 6*p*36*s*, 6*p*9*s*, 8*p*9*s*, 8*p*12*s*, 10*p*12*s*) are compared and analyzed. The detailed analysis results are shown in Fig. 8. The FEM and analytical calculation results of the six machines have very small errors, and the versatility and effectiveness of this model have been well proven.

3) Prototype experiment testing

To further verify the accuracy of this proposed analytical model, based on the aforementioned analysis and prototype data provided in Table I, a 6-pole 36-slot IPMSM equipped with the original rotor is manufactured for experiment testing. MTST-11A type machine test platform is shown in Fig. 9. Based on the motional electromotive force theory, the measurement experiment of flux density is carried out by pre-embedding wire in the stator teeth.

Hence, the air gap flux density can be calculated from the electromotive force E_{ew}, effective length L_{ew}, and speed n_0, namely

$$B_{test} = \frac{E_{ew}}{L_{ew} n_0} \tag{9}$$

Fig. 10 shows the comparison of the no-load back EMF obtained through the FEM and prototype test. Obviously, the results of the two methods are in good agreement. The 1th and 3th harmonic errors of the two methods are only 0.96% and 3.31%. The results of simulation analysis and experiment testing have been mutually verified.

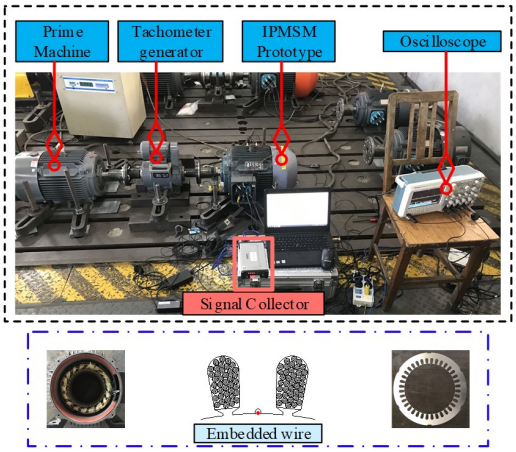

Fig. 9. Prototype test platform.

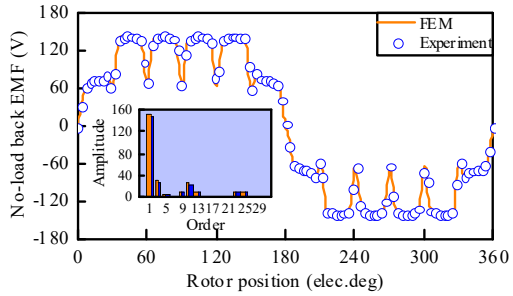

Fig. 10. Comparison of the no-load back EMF.

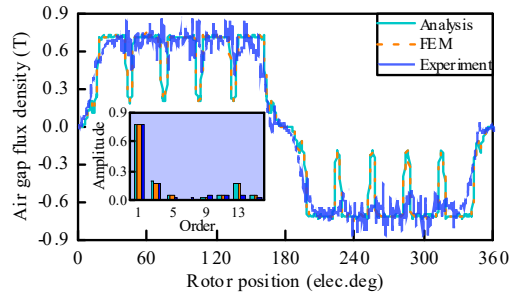

Fig. 11. Comparison of the air gap flux density.

The no-load air gap flux density distribution and harmonic content obtained through FEM, analytical method, and prototype test are shown in Fig. 11. It is not difficult to see that the harmonic components of air gap flux density obtained by the three methods are basically the same, and the experimental test results well verify the efficiency, accuracy, and practicability of this proposed model.

The stator cogging effect and the influence of complex boundary conditions of IPMSM can be well considered in this proposed analytical model to realize the rapid and accurate calculation of many electromagnetic characteristics, which provides favorable theoretical guidance for its characteristics improvement. In addition, this model is suitable for any other types of machines including IPMSM, and has high practical value and guiding significance.

III. Improvement Based on Different Combination of Pole Arc Coefficient

Considering that the electric drive system has higher requirements on the mechanical reliability and processing technology of its machine, based on the foregoing analysis, the electromagnetic improvement measure based on the different combination of pole arc coefficient is studied in detail in this section. This improvement measure can not only avoid the difficulty of manufacturing process caused by the stator skew slots, rotor skew poles, etc., but also eliminate the mechanical reliability problems caused by the unbalanced magnetic pulling force in the unequal pole arc coefficient and segmented skew poles. At the same time, it will not increase any cost and has important practical value.

When using different combination of pole arc coefficient, the distribution of equivalent permanent MMF $F_p(\theta)$ along the circumference is shown in Fig. 12. At this time, the Fourier expansion of $F_p^2(\theta)$ can be expressed as

$$F_p^2(\theta) = F_{p0} + \sum_{v=1}^{\infty} F_{pv} \cos vp\theta \tag{10}$$

where F_{p0} and F_{pv} represent the Fourier expansion coefficients.

$$\begin{aligned} F_{p0} &= \frac{F_a^2}{2}(\alpha_{pa} + \frac{\alpha_{pa}^2}{\alpha_{pb}}) \\ F_{pv} &= \frac{F_a^2}{v\pi}[\sin\frac{\alpha_{pa}}{2}v\pi + (-1)^v \frac{\alpha_{pa}^2}{\alpha_{pb}^2}\sin\frac{\alpha_{pb}}{2}v\pi] \end{aligned} \tag{11}$$

where α_{pa} and α_{pb} respectively represent the pole arc coefficients corresponding to two adjacent magnetic poles, F_a and F_b respectively represent their respective permanent MMF amplitudes. In addition, considering that the magnetic flux of each pole is equal, so $F_a\alpha_{pa}=F_b\alpha_{pb}$.

Combining (1), (7) and (10), the cogging torque analytical expression of the IPMSM with different combination of pole arc coefficient can be expressed as

$$T_{cog} = \frac{\mu_0 \pi z L_{ef}}{4}\left(R_{s2}^2 - R_{r1}^2\right)\sum_{j=1}^{\infty} j\Lambda_j F_v \sin jz\alpha \tag{12}$$

where j and v represent positive integers satisfying $v=jz/p$.

It can be seen from (11) that through reasonable configuration of different pole arc coefficient combinations, the jz/p^{th} Fourier coefficient F_{pv} (Especially lower order) of $F_p^2(\theta)$ can be effectively reduced, and the cogging torque can be effectively weakened. Taking a 6-pole 36-slot machine as an example, only the $12k$ (k is an integer) coefficient of $F_p^2(\theta)$ has an effect on its cogging torque. On the basis of ensuring that the pole arc coefficient α_p corresponding to an electrical cycle remains unchanged, the pole arc coefficient α_{pa} corresponding to one magnetic pole is an independent variable, and the other pole arc coefficient α_{pb} can be determined according to (13).

$$\begin{cases} \alpha_{pa} + \alpha_{pb} = 2\alpha_p \\ \dfrac{F_a^2}{12k\pi}[\sin\dfrac{\alpha_{pa}}{2}12k\pi + \dfrac{\alpha_{pa}^2}{\alpha_{pb}^2}\sin\dfrac{\alpha_{pb}}{2}12k\pi] = 0 \end{cases} \tag{13}$$

For the 6-pole 36-slot IPMSM for electric vehicles studied in this article, the pole arc coefficient α_p of one electrical cycle is 0.75. Based on this premise, three weakening tracks of the 12^{th}, 24^{th}, 36^{th} Fourier coefficient are shown in Fig. 13. It can be seen that different combinations have different weakening conditions for F_{p12}, F_{p24}, and F_{p36}. In order to achieve the best weakening effect, choose the combination of weakening lower order or weakening multiple lower orders at the same time as the optimal polar arc coefficient combination. For this machine,

the optimal combination of pole arc coefficients (α_{pa}: 0.667, α_{pb}: 0.833) can effectively weaken its cogging torque. A further comparative analysis of this pole arc combination will be made in the follow-up.

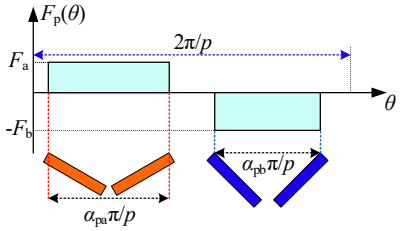

Fig. 12. Distribution of $F_p(\theta)$ for the improved machine.

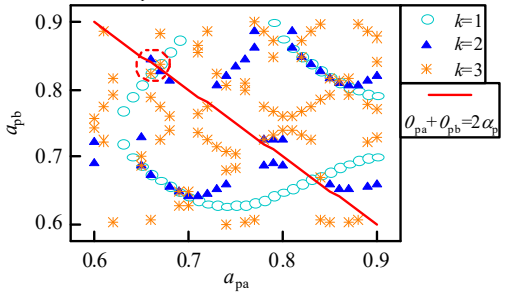

Fig. 13. Combination of the pole-arc coefficient.

IV. Machine Comprehensive Performance Evaluation

In order to study the impact of this improvement measure in the previous section on machine performance, the original machine (Motor 1), machine with rotor segmented skew poles (Motor 2), and machine with different combination of pole arc coefficient (Motor 3) are evaluated, including electromagnetic characteristics, vibration response, and mechanical strength performance. To ensure the comparison fairness, except for the difference in pole arc coefficient configuration and rotor assembly form, other machine configurations including amount of PMs are kept the same. It is worth noting that previous research work has shown that the 4-segment structure is a more reasonable choice for the machine with rotor segmented skew poles [23]. Therefore, 4-segment structure is adopted in the machine with rotor segmented skew poles in this study.

A. Comparison of Electromagnetic Characteristics

Fig. 14 and Table II show the cogging torque comparison of the three machines obtained by 3D FEM. It can be seen that the machine with different combination of pole arc coefficient has more excellent performance. Compared with Motor 1 and Motor 2, its peak cogging torque is reduced by 93.8% and 14.4%, respectively. It is worth noting that for integer slot PMSM, its tooth harmonic content of no-load back EMF is also one of the main sources of torque ripple, so it is particularly important to improve its back EMF waveform during the machine design stage. The no-load back EMF comparison of the three machines is shown in Fig. 15 and Table II. Compared with Motor 1 and Motor 2, the no-load back-EMF fundamental wave of Motor 3 has not only been significantly improved, but the third and above harmonics have also been effectively weakened and suppressed. Moreover, the total harmonic distortion (THD) of no-load back-EMF in Motor 3 calculated by (14) is improved by 52.6% and 24.0%, respectively, compared with the other two machines.

$$THD = \sqrt{(\sum_{n=2}^{\infty} E_n^2)} / E_1 \tag{14}$$

where E_1 and E_n represent the effective value of the fundamental wave and the n^{th} harmonic of no-load back EMF.

Table II also shows the electromagnetic characteristics of the three machines under rated load. Detailed torque curves are shown in Fig. 16. It can be seen that the machine with different combination of pole arc coefficient still have excellent load electromagnetic performance. Compared with the other two machines, not only the average torque in Motor 3 has been improved, but its torque ripple has also been reduced by 81.3% and 6.2%, respectively. This shows that the excellent no-load characteristics in Motor 3 have further affected its load characteristics, especially the large reduction in torque ripple. For the IPMSM used in electric vehicles, low torque ripple can not only meet the high-performance requirements of electric drive systems, but also help improve its electromagnetic vibration characteristics. Therefore, Motor 3 has higher engineering practical value than the other two machines.

Furthermore, the unbalanced magnetic pulling force of the three machines is analyzed by FEM, and the analysis results are shown in Table II. It can be seen that machine with rotor segmented skew poles has a large axial unbalanced magnetic pulling force, which has a serious impact on the life and overall performance of the machine.

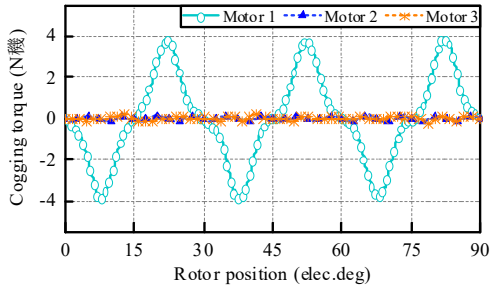

Fig. 14. Comparison of the cogging torque.

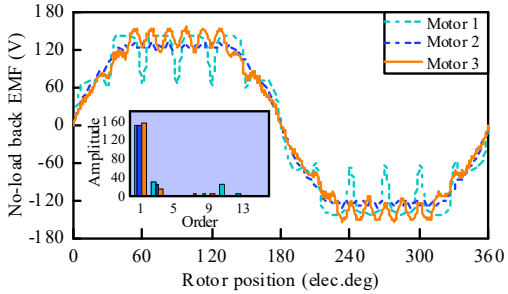

Fig. 15. Comparison of the no-load back EMF.

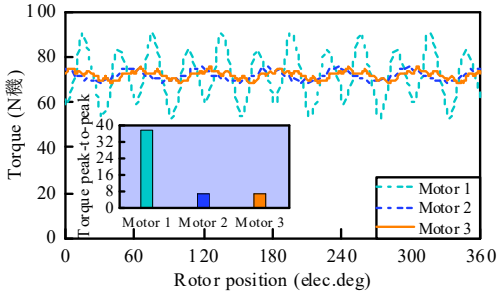

Fig. 16. Comparison of the on-load torque.

TABLE II
THE KEY DATA OF MAIN ELECTROMAGNETIC CHARACTERISTICS

Item	Symbol (unit)	Motor 1	Motor 2	Motor 3
Cogging torque	Pk-Pk (N·m)	7.659	0.473	0.414
No-load back EMF	1^{th} (V)	149.4	147.8	155.6
	3^{th} (V)	29.3	26.5	16.1
	11^{th} (V)	25.3	2.3	1.4
	13^{th} (V)	7.8	0.8	0.5
On-load torque	T_{avg} (N·m)	71.71	71.72	71.97
	T_{rip} (%)	52.8	10.5	9.9
	T_{max} (N·m)	90.71	75.94	75.54
	T_{min} (N·m)	52.86	68.40	68.44
Unbalanced magnetic force	F_r (N)	0.00	0.00	0.00
	F_z (N)	0.00	7.56	0.00

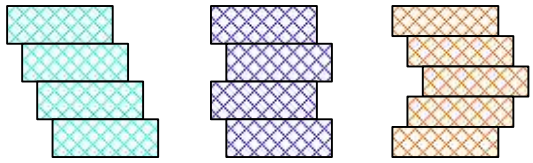

Fig. 17. Different rotor segmented skew poles structures.

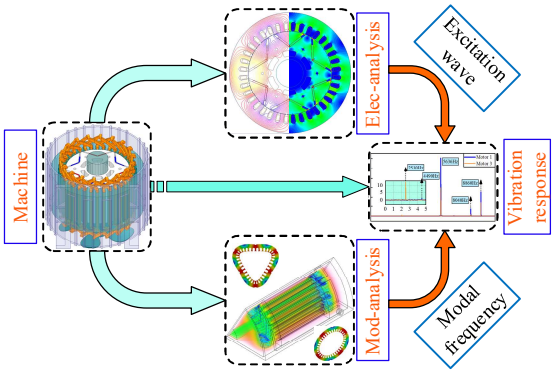

Fig. 18. Vibration response multi-physics analysis process.

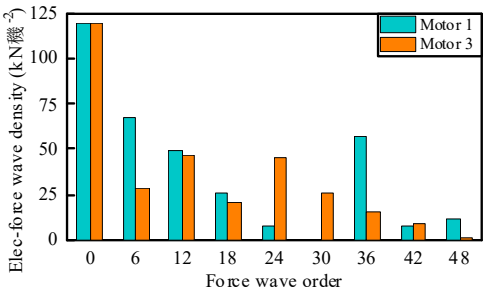

Fig. 19. Comparison of the electromagnetic force wave.

In addition, the unbalanced magnetic pulling force of different rotor segmented skew poles structures (as shown in Fig. 17) cannot be effectively eliminated either. At the same time, this structure has extremely high requirements for processing technology and mechanical strength, especially when used in high-performance applications such as electric vehicles. Therefore, the advantages and value of Motor 3 in electric vehicles are more obvious.

B. Comparison of Vibration Response

Fig. 18 shows the multi-physics analysis process of the machine vibration response. Firstly, the radial electromagnetic force wave calculated by FEM is shown in Fig. 19. The results show that, compared with Motor 1, Motor 3 can weaken some specific order electromagnetic force waves, especially the 6^{th}, 12^{th}, and 18^{th} force waves, and its weakening effect is as high as 57.8%, 5.2%, 20.9%. Although it cannot completely weaken or eliminate all order force waves, the effective weakening of low-order force waves still proves the effectiveness of Motor 3 in improving electromagnetic vibration characteristics.

Secondly, to avoid the influence of machine resonance on the operation stability of electric drive system, a 3D stator model is established, and its modal shape and natural frequency are analyzed and calculated by FEM. Detailed results are shown in Fig. 20. It will be used in the harmonic response analysis field together with electromagnetic force waves to realize the calculation of machine vibration response.

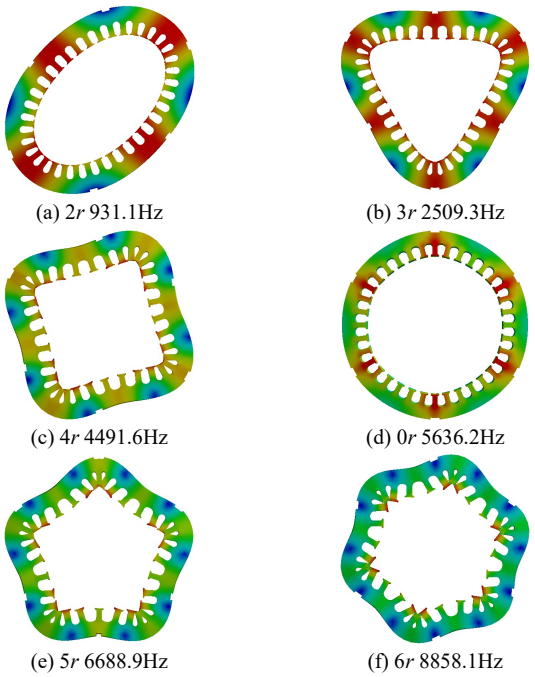

Fig. 20. Modal shape and natural frequency of the stator core.

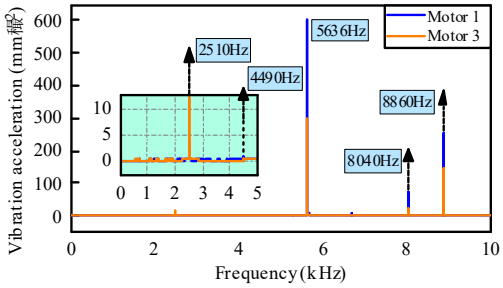

Fig. 21. Comparison of the vibration acceleration response.

Finally, the vibration response is calculated by the mode shape superposition method, as shown in Fig. 21. It can be seen that, compared with original machine, the vibration response of Motor 3 is better. Its vibration acceleration amplitude at key frequency points has been significantly improved. This result once again proves that Motor 3 has a better vibration level. Compared with Motor 1, it has better NVH performance without increasing the cost and processing difficulty.

C. Comparison of Mechanical Strength

The rotor configuration of the machine with different combination of pole arc coefficient has changed the mechanical

structure in original machine to a certain extent. Small changes often affect the stress concentration performance, especially the rotor ribs and magnetic isolation bridge area. In addition, IPMSM for electric vehicles need to face various complex working conditions, so it is essential to analyze its mechanical strength. Fig. 22 shows the multi-physics analysis process of the mechanical strength. The temperature distribution calculated through the coupling of electromagnetic and temperature field also acts on the rotor as a load (thermal stress), thereby obtaining a more accurate mechanical strength performance. Four mechanical strength characteristics of Motor 1 and Motor 3, including rotor equivalent stress, strain, radial stress, and tangential stress, are analyzed. Detailed results are shown in Fig. 23.

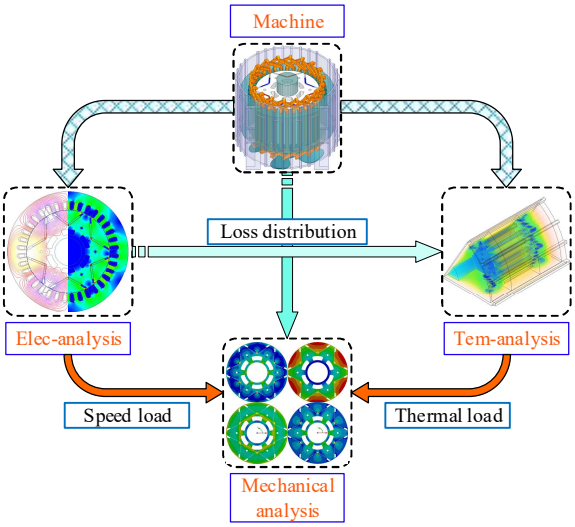

Fig. 22. Mechanical strength multi-physics analysis process.

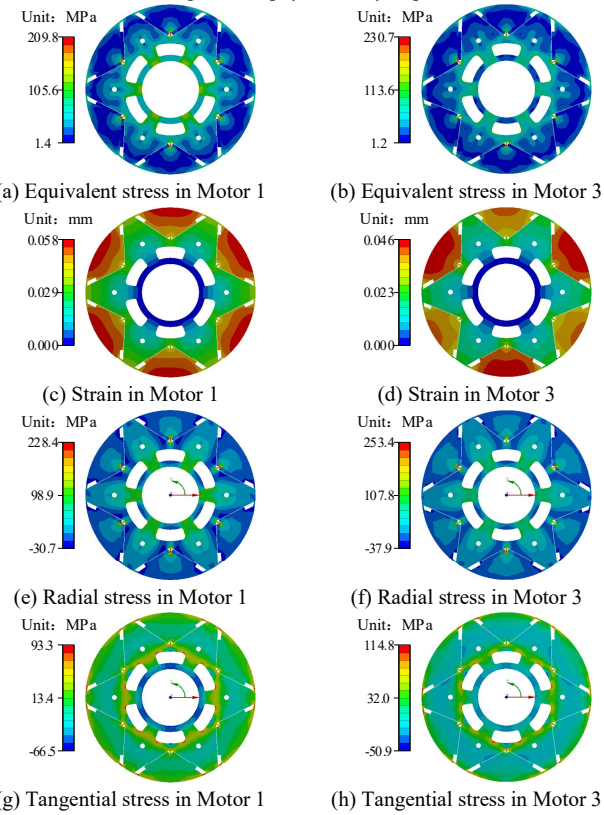

(a) Equivalent stress in Motor 1 (b) Equivalent stress in Motor 3

(c) Strain in Motor 1 (d) Strain in Motor 3

(e) Radial stress in Motor 1 (f) Radial stress in Motor 3

(g) Tangential stress in Motor 1 (h) Tangential stress in Motor 3

Fig. 23. Comparison of the mechanical strength analysis.

It can be seen that the maximum equivalent stresses of Motor 1 and Motor 3 appear on the magnetic isolation bridge, respectively, 209.8MPa and 230.7MPa, which are far less than the material yield limit (405MPa), and the maximum deformation is 0.058mm and 0.046mm respectively. The results show that the rotor structures of the machine with different combination of pole arc coefficient still meet the mechanical requirements.

V. Conclusion

In this article, a universal magnetic field analytical model for the IPMSM is first proposed, which can realize the rapid prediction of key electromagnetic characteristics such as cogging torque, air gap flux density, and exciting force wave. After that, based on this model, the improvement measure of different combination of pole arc coefficient on cogging torque and electromagnetic vibration are studied. Finally, a comprehensive comparative analysis of the electromagnetic characteristics, vibration response, and mechanical strength performance is carried out. The following conclusions can be drawn:

1) The proposed model can quickly and accurately calculate the equivalent permanent MMF and air gap permeance (effective air gap length), and then realize the solution of other key electromagnetic characteristics. Its universality, accuracy, and practicability have been proven through three magnetic pole structures (U-shaped, V-shaped, One-shaped), six pole-slot combinations (4*p*36*s*, 6*p*36*s*, 6*p*9*s*, 8*p*9*s*, 8*p*12*s*, 10*p*12*s*), and prototype experiments.

2) Based on the above model, the cogging torque calculation formula of the machine different combination of pole arc coefficient is derived, and then the optimal pole arc coefficient combination is calculated to improve its electromagnetic characteristics.

3) Compared with Motor 1 and Motor 2, Motor 3 can significantly weaken the THD of no-load back EMF, cogging torque, and torque ripple, and has very excellent electromagnetic characteristics. At the same time, compared with Motor 2, there is no need to consider issues such as processing technology, cost, and vicious unbalanced magnetic pulling force.

4) Some specific orders of electromagnetic force waves can be effectively weakened in Motor 3, especially the 6th, 12th, and 18th force waves, and its weakening effect is as high as 57.8%, 5.2%, 20.9%. It has a very superior vibration response, and the vibration acceleration amplitude at some key frequency points has a significant drop. Compared with original machine, the maximum value of vibration acceleration amplitude decreased from 604.6mm/s^2 to 295.1mm/s^2, a decrease of 51.2%.

References

[1] E. Bostanci, M. Moallem, A. Parsapour and B. Fahimi, "Opportunities and Challenges of Switched Reluctance Motor Drives for Electric Propulsion: A Comparative Study," *IEEE Transactions on Transportation Electrification*, vol. 3, no. 1, pp. 58-75, Mar. 2017.

[2] A. Emadi, Y. J. Lee and K. Rajashekara, "Power Electronics and Motor Drives in Electric, Hybrid Electric, and Plug-In Hybrid Electric Vehicles,"

IEEE Transactions on Industrial Electronics, vol. 55, no. 6, pp. 2237-2245, Jun. 2008.

[3] S. K. Kommuri, M. Defoort, H. R. Karimi and K. C. Veluvolu, "A Robust Observer-Based Sensor Fault-Tolerant Control for PMSM in Electric Vehicles," *IEEE Transactions on Industrial Electronics*, vol. 63, no. 12, pp. 7671-7681, Dec. 2016.

[4] Feng Chai, Shumei Cui and Shukang Cheng, "Performance analysis of double-stator starter generator for the hybrid electric vehicle," *IEEE Transactions on Magnetics*, vol. 41, no. 1, pp. 484-487, Jan. 2005.

[5] C. Feng, X. Jing, G. Bin, C. Shukang and Z. Jiange, "Double-Stator Permanent Magnet Synchronous in-Wheel Motor for Hybrid Electric Drive System," *IEEE Transactions on Magnetics*, vol. 45, no. 1, pp. 278-281, Jan. 2009.

[6] D. Fodorean, M. M. Sarrazin, C. S. Marţiş, J. Anthonis and H. Van der Auweraer, "Electromagnetic and Structural Analysis for a Surface-Mounted PMSM Used for Light-EV," *IEEE Transactions on Industry Applications*, vol. 52, no. 4, pp. 2892-2899, Jul./Aug. 2016.

[7] J. Jung, S. Lee, G. Lee, J. Hong, D. Lee and K. Kim, "Reduction Design of Vibration and Noise in IPMSM Type Integrated Starter and Generator for HEV," *IEEE Transactions on Magnetics*, vol. 46, no. 6, pp. 2454-2457, Jun. 2010.

[8] X. Liu, H. Chen, J. Zhao and A. Belahcen, "Research on the Performances and Parameters of Interior PMSM Used for Electric Vehicles," *IEEE Transactions on Industrial Electronics*, vol. 63, no. 6, pp. 3533-3545, Jun. 2016.

[9] E. Severson, R. Nilssen, T. Undeland and N. Mohan, "Magnetic Equivalent Circuit Modeling of the AC Homopolar Machine for Flywheel Energy Storage," *IEEE Transactions on Energy Conversion*, vol. 30, no. 4, pp. 1670-1678, Dec. 2015.

[10] Chuntao Chen, Xinzhen Wu, Xiaoqin Zheng and Shenghua Zhao, "Analytical Calculation of Air-Gap Magnetic Field of Permanent-Magnet Motor Based on Improved Equivalent Surface Current Method," *Proceedings of the CSEE*, [online], pp. 1-10, Sep. 2021.

[11] P. Liang, F. Chai, Y. Li and Y. Pei, "Analytical Prediction of Magnetic Field Distribution in Spoke-Type Permanent-Magnet Synchronous Machines Accounting for Bridge Saturation and Magnet Shape," *IEEE Transactions on Industrial Electronics*, vol. 64, no. 5, pp. 3479-3488, May 2017.

[12] Z. Q. Zhu, L. J. Wu and Z. P. Xia, "An Accurate Subdomain Model for Magnetic Field Computation in Slotted Surface-Mounted Permanent-Magnet Machines," *IEEE Transactions on Magnetics*, vol. 46, no. 4, pp. 1100-1115, Apr. 2010.

[13] J. Ren, X. Wang and W. Zhao, "Magnetic Field Prediction of the Saturated Surface-mounted Permanent Magnet Synchronous Machine with Rotor Eccentricity," *IEEE Transactions on Industrial Electronics*, doi: 10.1109/TIE.2021.3105985.

[14] A. M. EL-Refaie, "Fractional-Slot Concentrated-Windings Synchronous Permanent Magnet Machines: Opportunities and Challenges," *IEEE Transactions on Industrial Electronics*, vol. 57, no. 1, pp. 107-121, Jan. 2010.

[15] D. Wang, X. Wang, D. Qiao, Y. Pei and S. Jung, "Reducing Cogging Torque in Surface-Mounted Permanent-Magnet Motors by Nonuniformly Distributed Teeth Method," *IEEE Transactions on Magnetics*, vol. 47, no. 9, pp. 2231-2239, Sep. 2011.

[16] K. Wang, Z. Q. Zhu, G. Ombach and W. Chlebosz, "Average Torque Improvement of Interior Permanent-Magnet Machine Using Third Harmonic in Rotor Shape," *IEEE Transactions on Industrial Electronics*, vol. 61, no. 9, pp. 5047-5057, Sep. 2014.

[17] D. Wang, X. Wang, Y. Yang and R. Zhang, "Optimization of Magnetic Pole Shifting to Reduce Cogging Torque in Solid-Rotor Permanent-Magnet Synchronous Motors," *IEEE Transactions on Magnetics*, vol. 46, no. 5, pp. 1228-1234, May 2010.

[18] Xiuhe Wang, Yubo Yang, Tingting Ding, Changqing Zhu and Daohan Wang, "The Method for Reducing Cogging Torque by Suitable Selection of Pole-Arc Coefficient in Solid-Rotor PM Synchronous Motors," *Proceedings of the CSEE*, vol. 25, no. 15, pp. 146-149, Aug. 2005.

[19] Z. Xing, X. Wang and W. Zhao, "Research on Weakening Measure of Radial Electromagnetic Force Waves in Permanent Magnet Synchronous Motors by Inserting Auxiliary Slots," *IET Electric Power Applications*, vol. 14, no. 8, pp. 1381-1395, Aug. 2020.

[20] C. Peng, D. Wang, Z. Feng and B. Wang, "A New Segmented Rotor to Mitigate Torque Ripple and Electromagnetic Vibration of Interior Permanent Magnet Machine," *IEEE Transactions on Industrial Electronics*, doi: 10.1109/TIE.2021.3063869.

[21] Mengjia Jin, Weizhong Fei and Jianxin Shen, "Investigation of Axial Magnetic Force in Permanent Magnet Synchronous Machines with Rotor Step Skewing," *Journal of Electrical Engineering*, vol. 28, no. 11, pp. 19-27, Nov. 2013.

[22] C. Ma and S. Zuo, "Black-Box Method of Identification and Diagnosis of Abnormal Noise Sources of Permanent Magnet Synchronous Machines for Electric Vehicles," *IEEE Transactions on Industrial Electronics*, vol. 61, no. 10, pp. 5538-5549, Oct. 2014.

[23] Z. Xing, X. Wang and W. Zhao, "Cogging Torque Reduction Based on Segmented Skewing Magnetic Poles with Different Combinations of Pole-Arc Coefficients in Surface-Mounted Permenent Magnet Synchronous Motors," *IET Electric Power Applications*, vol. 15, no. 2, pp. 200-213, Feb. 2021.

Feng Liu was born in China on November 1997. He received the B.E. degree in electrical engineering from Qingdao University, Qingdao, China, in 2020. He is currently working toward the Ph.D. degree in the School of Electrical Engineering, Shandong University, Jinan, China.

His current research interests include design and analysis of permanent magnet machines, motor drive and control on electric vehicle.

Xiuhe Wang (Member, IEEE) was born in China on July 1967. He received the B.E. and M.E. degrees in electrical engineering from Shandong University, Jinan, China, in 1989 and 1993, respectively, and the Ph.D. degree in electrical engineering from Shenyang University of Technology, Shenyang, China, in 1996.

From 2001 to 2002, he was a Postdoctoral Fellow with Seoul National University, Seoul, South Korea. Since 2000, he has been a Professor with the School of Electrical Engineering, Shandong University, Jinan, China. His research interests include permanent magnet machines, theoretical analysis and calculation of electromagnetic devices, and artificial intelligence and its application on electrical machines. He has authored/coauthored more than 100 papers on these topics.

Zezhi Xing was born in China on August 1994. He received the B.E. degree from the Shenyang University of Technology, Shenyang, China, in 2016, and the M.E. degree from Shandong University, Jinan, China, in 2019. He is currently working toward the Ph.D. degree in the School of Electrical Engineering, Shandong University, Jinan, China.

His current research interests include design and analysis of the special electrical machines, electromagnetic vibration and control.

Aiguo Yu was born in China on January 1965. He received the B.E. degree in electrical engineering from Shandong University, Jinan, China, in 1989. He is currently working for Qingdao Haidian Electric Co., Ltd. as the executive vice president, chief engineer, and senior engineer.

His current research interests include research and development of power transformers and other power distribution equipment.

Changbin Li was born in China on December 1996. He received the B.E. degree in electrical engineering from Shandong University of Science and Technology, Qingdao, China, in 2020. He is currently working toward the M.E. degree in the School of Electrical Engineering, Shandong University, Jinan, China.

His current research interests include design and analysis of permanent magnet-assisted synchronous reluctance motor, motor drive and control on electric vehicle.